COMPLETE NOISE ANALYSIS FOR CMOS SWITCHING MIXERS VIA STOCHASTIC DIFFERENTIAL EQUATIONS

Donhee Ham and Ali Hajimiri

California Institute of Technology, Pasadena, CA 91125, USA

ABSTRACT

A complete analysis of noise in CMOS switching mixers using stochastic differential equations (SDE) is presented. The noise figure is calculated using this analysis which takes both cyclostationary noise sources and capacitive high frequency effects into account. The analysis leads to important design implications for mixer design and shows that some commonly-used approximations for mixer noise calculations can be misleading in certain cases even at low frequencies. It is demonstrated that there is an optimum value for the load capacitor leading to minimum noise figure and maximum conversion gain for the mixer.

1. INTRODUCTION

Accurate prediction of mixer noise is complicated due to time variance of elements, cyclostationary noise sources and high frequency effects. Although a complete time-domain technique based on time varying impulse responses exists [1], it is very time consuming as it requires multiple simulation runs to numerically calculate the noise for a given topology of mixers. Although insightful parametric expressions for mixer noise figure [2] can be obtained by ignoring the high frequency capacitive effects, those expressions can lead to large errors at high frequencies. Stochastic differential equations (SDE) have been applied to mixer noise analysis to include the capacitive effect and time-varying properties of mixers [3] without calculating the cyclostationary effects leading to inaccurate results.

In this work, we consider the cyclostationary noise generation in the presence of capacitances. SDEs are used to obtain autocorrelation functions of the output noise voltage, whose power spectral density (PSD) is periodic due to cyclostationarity effects. The dynamics of mixer noise generation is modeled in time-domain using the time-varying PSD, which facilitates a comparison between stationary and cyclostationary noise calculations. The dependence of the PSD on capacitances and switching modes provides further insight to the mixer design by identifying an optimum capacitance for minimum noise figure and maximum conversion gain. This approach lends itself very well to computer simulations, resulting in fast calculation of noise figure of mixers.

In Sec. 2, we describe the CMOS switching mixers operation and obtain an expression for the conversion gain, which will be used to calculate input-referred noise later. SDEs describing mixer noise are derived and solved in Sec. 3. Numerical examples and the design implications appear in Sec. 4.

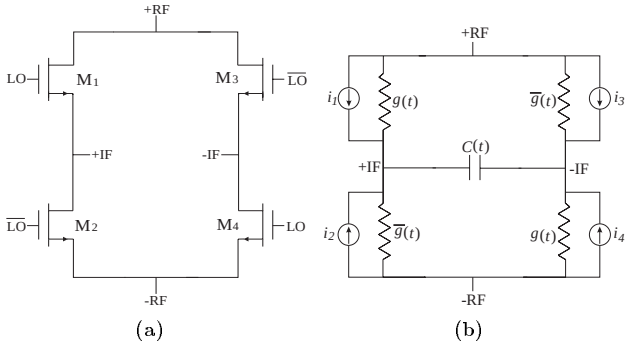

Figure 1: (a) Schematic (b) RC-model and noise sources

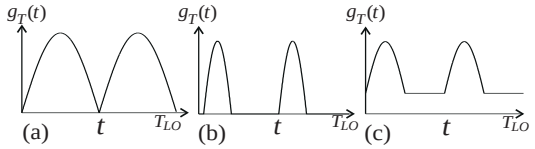

Figure 2: Three switching modes and $g_T(t)$: (a) zero-overlap (b) off-overlap (c) on-overlap

2. CMOS SWITCHING MIXERS AND CONVERSION GAIN

The switching mixer topology and its equivalent RC-network model including noise sources are shown in Fig. 1. Although it is possible to account for non-zero RF port resistance in this topology [4], in this paper, we only consider the zero resistance case to avoid cumbersome mathematical expressions. Hence, input-referred noise will be used as a figure of merit in the following sections.

Transistors M_1 and M_4 are driven by the local oscillator, f_{LO}, and M_2 and M_3 are driven by the opposite phase of LO. $g(t)$ and $\overline{g}(t)$ represent channel conductances of MOS transistors which are periodic in f_{LO} and are 180° out of phase. The dc voltage difference between RF input port is assumed to be small to guarantee switching between off and deep triode region, which is true in most practical cases as the RF and IF signals are generally small. In triode region, the channel conductance of MOS transistors are given by

$$g(t) \quad = \quad \mu_n C_{ox} \frac{W}{L} [V_{gs}(t) - V_{ds}(t) - V_{th}(t)] \qquad (1)$$

where the time-variant threshold voltage accounts for the body effect of the MOS transistors.

The conversion gain can be calculated using superposition integral of impulse response functions as in [5]. However, we derive the relation between $v_{rf}(t)$ and $v_{if}(t)$ by solving the following differential equation obtained from KCL in Fig. 1(b), *i.e.*,

$$C(t)\frac{dv_{if}(t)}{dt} + [g_T(t) + \frac{dC(t)}{dt}]v_{if}(t) = m(t)g_T(t)v_{rf}(t) \quad (2)$$

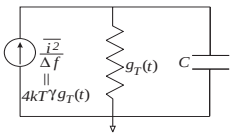

Figure 3: A simple model for noise sources and the switching mixer

The load capacitance, $C(t)$, is usually time-varying as it consists of the input capacitance of the next stage and parasitics of the mixer core. The two periodic functions, $m(t)$ and $g_T(t)$ are defined as

$$m(t) = \frac{g(t)-\overline{g}(t)}{g(t)+\overline{g}(t)} \quad (3)$$

$$g_T(t) = \frac{g(t)+\overline{g}(t)}{2} \quad (4)$$

It can be easily seen that the mixing function, $m(t)$, and the effective conductance, $g_T(t)$ have fundamental frequencies of f_{LO} and $2f_{LO}$, respectively. As typical waveforms of $g_T(t)$ in Fig. 2 show, there are three different switching modes. Fig. 2(a) shows the zero-overlap case where M_1 - M_4 pair turns on immediately after M_2 - M_3 pair turns off and vice versa. Fig. 2(b) shows the off-overlap case where there is a period of time when all transistors are off leaving the IF port floating. The on-overlap case is shown in Fig. 2(c), where all transistors are on for a fraction of the period. It is well known that the switching mode of the mixer affects its performance [5].

In the case of no load capacitances, (2) reduces to :

$$v_{if}(t) = m(t)v_{rf}(t) \quad (5)$$

and the conversion gain is simply $M(f_{LO})$ where $M(f)$ is the Fourier transformation of $m(t)$. Full conversion gain analysis with capacitances can be performed by solving (2). Noting that $\Phi(t) \equiv \int_0^t C^{-1}(t')[g_T(t')+(d/dt')C(t')]dt'$ is an argument of the integrating factor for (2) [6], the following solution for $v_{if}(t)$ can be obtained :

$$v_{if}(t) = e^{-\Phi(t)} \int_0^t e^{\Phi(t')} m(t') g_T(t') C^{-1}(t') v_{rf}(t') dt' \quad (6)$$

with an initial condition of $v_{if}(0) = 0$. We are interested in $v_{if}(t)$ at large ts. This integral can be numerically evaluated to calculate the conversion gain of the mixer. Two examples are given in Sec. 4.

3. MIXER NOISE ANALYSIS VIA SDE

In this section, we derive and solve a SDE for switching mixers to investigate cyclostationary effects in the presence of load and parasitic capacitances. With the RF port at ground in Fig. 1(b), KCL and superposition result in the following SDE for the noisy voltage $v(t)$ across the capacitor $C(t)$:

$$C(t)\frac{dv(t)}{dt} + [g_T(t) + \frac{dC(t)}{dt}]v(t) = \frac{1}{2}(i_1+i_2-i_3-i_4) \quad (7)$$

Assuming that all the noise sources are uncorrelated since they are generated by different transistors, we have

$$\frac{1}{4}\frac{\overline{(i_1+i_2-i_3-i_4)^2}}{\Delta f} = 4kT\gamma g_{0T}(t) \quad (8)$$

where $g_{0T}(t)$ is $g_T(t)$ given by (4) for $V_{ds}(t) = 0$.

The right hand side of (7) is cyclostationary and can be expressed as the product of a stationary noise source $i_0(t)$ and a deterministic noise modulating function (NMF), $\alpha(t)$ [7]:

$$\frac{1}{2}(i_1+i_2-i_3-i_4) = i_0(t)\alpha(t) \quad (9)$$

where $\overline{i_0^2}/\Delta f = 4kT\gamma g_{0T,max}$ and $\alpha^2(t) = g_{0T}(t)/g_{0T,max}$. The above decomposition of the cyclostationary noise sources reduces (7) to :

$$\frac{dv(t)}{dt} + \omega(t)v(t) = \frac{\alpha(t)}{C(t)}i_0(t) \quad (10)$$

where $\omega(t) \equiv C^{-1}(t)[g_T(t) + (d/dt)C(t)]$.

We assume an initial condition of $v(0) = 0$ for (10) and we are interested in large ts when the initial transient fades out. The autocorrelation function of $v(t)$ can be obtained through two steps. First, by multiplying (10) at t_2 by $i_0(t_1)$ and taking the expected value, we obtain

$$\frac{\partial}{\partial t_2}R_{i_0,v}(t_1,t_2) + \omega(t_2)R_{i_0,v}(t_1,t_2) = \frac{\alpha(t_2)}{C(t_2)}R_{i_0,i_0}(t_1,t_2) \quad (11)$$

with an initial condition of $R_{i_0,v}(t_1,0) = 0$. Second, by multiplying (10) at t_1 by $v(t_2)$ and taking the expected value, we obtain

$$\frac{\partial}{\partial t_1}R_{v,v}(t_1,t_2) + \omega(t_1)R_{v,v}(t_1,t_2) = \frac{\alpha(t_1)}{C(t_1)}R_{i_0,v}(t_1,t_2) \quad (12)$$

with an initial condition of $R_{v,v}(0,t_2) = 0$. Exploiting $R_{i_0,i_0}(t_1,t_2) = \sigma_{i_0}^2\delta(t_1-t_2)$ for white noise where $\sigma_{i_0}^2 = 4kT\gamma g_{0T,max}$ and hiring the integrating factor technique [6], we obtain

$$R_{i_0,v}(t_1,t_2) = \sigma_{i_0}^2 \frac{\alpha(t_1)}{C(t_1)} e^{[\Phi(t_1)-\Phi(t_2)]}u(t_2-t_1) \quad (13)$$

where $u(t)$ is the unit step function. By plugging (13) to (12) and using the integrating factor technique again [6], we obtain the autocorrelation function of the noise voltage at the IF-port :

$$R_{v,v}(t_1,t_2) = \sigma_{i_0}^2 e^{-[\Phi(t_1)+\Phi(t_2)]} \int_0^{min(t_1,t_2)} [\frac{\alpha(t)}{C(t)}]^2 e^{2\Phi(t)}dt \quad (14)$$

This is the most general form of the autocorrelation function from which the PSD is calculated numerically.

Although evaluating (14) is possible numerically [4], we make two simplifying assumptions to gain more insight. Since V_{ds} is generally very small due to the weak IF and RF signals, $g_T(t) \approx g_{0T}(t)$. This deep-triode approximation and equations (7) and (8) imply that Fig. 3 can be used to model noise. Also, the time-varying capacitance, $C(t)$, is approximated with a constant capacitance C. These two approximations reduce (14) to :

$$R_{v,v}(t_1,t_2) = \frac{\sigma_{i_0}^2}{2Cg_{0T,max}}[e^{-|\Phi(t_1)-\Phi(t_2)|} - e^{-[\Phi(t_1)+\phi(t_2)]}] \quad (15)$$

As $dC/dt = 0$ and hence $\omega(t) = g_T(t)/C$ is positive, the second term will die out for large ts in $R_{v,v}(t+\tau,t)$. Therefore, (15) further reduces to

$$R_{v,v}(t+\tau,t) = \frac{2kT\gamma}{C}\exp[-\left|\int_t^{t+\tau}\omega(t)dt\right|] \quad (16)$$

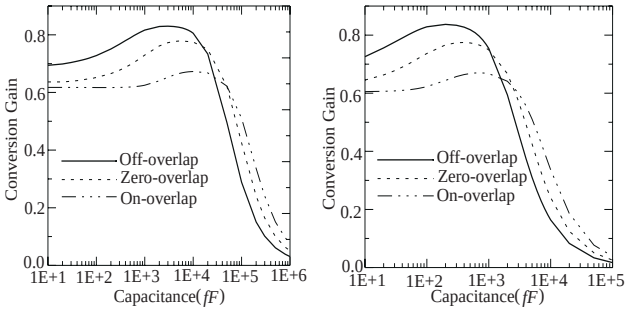

Figure 4: Conversion gain vs. cap. (a) f_{RF}=200MHz, f_{LO}=190MHz (b) f_{RF}=2.44GHz, f_{LO}=2.24GHz

As a special case, neglecting all the high frequency terms of $g_T(t)$ except its dc component, g_0, the argument of the *exp* in (16) reduces to $-\frac{g_0}{C}|\tau|$ and hence

$$S_{v0}(f) = \frac{4kT\gamma g_0}{g_0^2 + 4\pi^2 f^2 C^2} \quad (17)$$

which is the same result obtained from the equivalent circuit of Fig. 3 with a constant $g_T(t)$. As will be seen in the following section, ignoring cyclostationarity and frequency-dependence as in (17) can lead to gross errors in the estimated noise depending on capacitance values and switching modes.

4. SIMULATION RESULTS AND DESIGN IMPLICATIONS

Trapezoidal integration algorithm is used to calculate the output PSD at f_{IF} using (16). The PSD is a periodic function of time since the noise sources are cyclostationary and their fundamental frequency is $2f_{LO}$. To emphasize the time-varying nature of PSD at f_{IF}, we will denote it as $S(f_{IF}, t)$. To investigate the dynamics of noise generation and design implications for different capacitance values and switching modes, two different examples are considered :

4.1. f_{LO}=190MHz, f_{RF}=200MHz, and f_{IF}=10MHz

The conversion gain obtained from (6) with various constant capacitance values is depicted in Fig. 4(a). As noted in [5], the conversion gain can be larger than $2/\pi$ in the presence of capacitors, as shown in Fig. 4. The increase in conversion gain stops and reverses once the effective 3dB frequency of the mixer becomes comparable to $2\pi f_{IF}$, *i.e.*,

$$C_{conv} \approx \frac{g_0}{2\pi f_{IF}} \quad (18)$$

The conversion gain begins decreasing as the f_{IF} components are filtered out as well. Therefore, there exists an optimal capacitance resulting in maximum conversion gain.

Fig. 5 shows $S(f_{IF}, t)$ at the IF port for off-overlap, zero-overlap and on-overlap switching modes for different IF capacitances. As mentioned earlier, $S(f_{IF}, t)$ is periodic in $2f_{LO}$. Regardless of the switching type, the noise at the IF port is boosted when $g_T(t)$ is small and attenuated when $g_T(t)$ is large. Also a smaller capacitance results in larger variations in the PSD while a larger capacitance averages out more of $2f_{LO}$ cyclostationarity and reduces the time-variations of the PSD.

In the off-overlap switching mode, noise at IF is large when all the transistors are off and IF port floats. The voltage stored on the capacitor stays constant and thus the

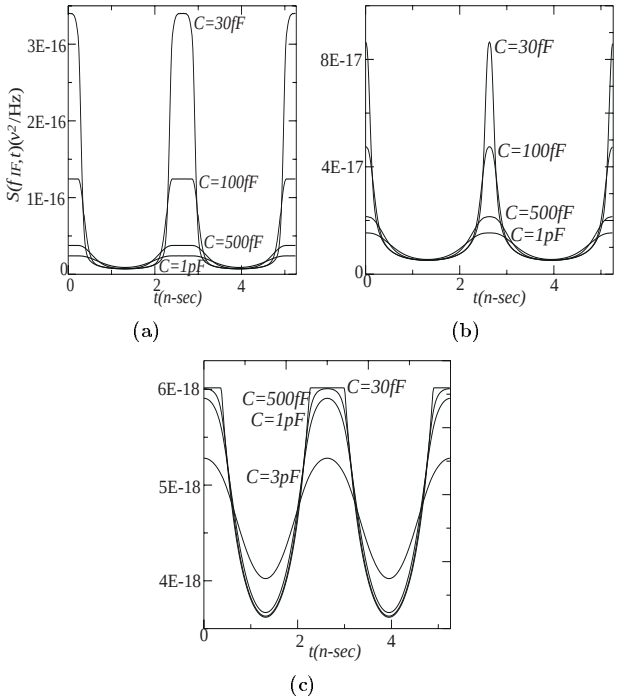

Figure 5: $S(f_{IF}, t)$ for f_{RF}=200MHz, f_{LO}=190MHz : (a) off-overlap (b) zero-overlap (c) on-overlap

spectral density of the IF noise remains the same, which explains the plateaux observed in Fig. 5(a). For a small capacitance, most of the total noise is introduced during this plateau, *e.g.*, for $C = 30fF$ and $C = 100fF$, the plateaux are 15dB and 11dB higher than the flat valley, respectively. Thus, for small capacitances, the large noise generation during the off-period makes the time-averaged PSD, $< S_v(f_{IF}, t) >$, deviate to a great extent from the stationary PSD, $S_{v0}(f_{IF})$, as seen in Table 1. For $C = 30fF$ and $C = 100fF$, deviations are 8.1dB and 5.2dB, respectively. Thus, a blind application of (17) to the mixer noise calculation can result in large errors. As the capacitance becomes larger and the approximate effective bandwidth, g_0/C approaches $2\pi \times 2f_{LO}$, the cyclostationary effects will be filtered out, lowering the height of plateaux and hence $< S_v(f_{IF}, t) >$ approaches $S_{v0}(f_{IF})$. A simplified, yet insightful way of looking at this effect is by noting that the mean square noise voltage on the capacitor in a sampling switch is given by kT/C which increases for smaller values of C.

For the zero-overlap switching shown in Fig. 5(b), the noise at IF is large close to on-off transition of the transistors. Since the noise boosting is not as strong as in the off-overlap switching, the difference between $< S_v(f_{IF}, t) >$ and $S_{v0}(f_{IF})$ is not as large but still considerable for small capacitances as shown in Table 1.

For the on-overlap switching, the time-variance of the PSD is significantly weaker when compared to the other two switching modes as shown in Fig. 5(c) and $S_{v0}(f_{IF})$ can be used as a good approximation for $< S_v(f_{IF}, t) >$ in most cases as seen in Table 1. The difference in the PSD between on- and off-overlap cases is considerable, and amounts to 12.6dB and 9.6dB for $C = 30fF$ and $C = 100fF$, respectively.

Assuming zero RF port impedance [4] to obtain insight, the input-referred RF-port noise becomes a more appropriate figure of merit. In Fig. 6(a), we plot the RF-port-

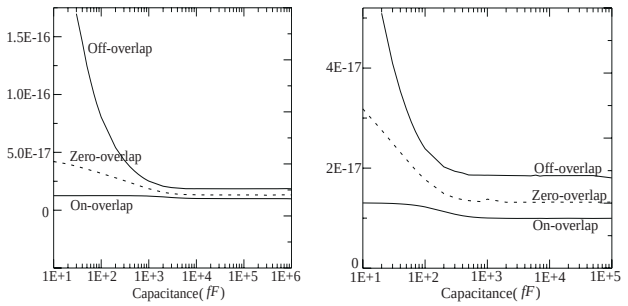

(a) (b)

Figure 6: RF-port PSD(v^2/Hz) vs. cap. (a) f_{RF}=200MHz, f_{LO}=190MHz (b) f_{RF}=2.44GHz, f_{LO}=2.24GHz

referred noise as a function of capacitance for the three switching modes, showing the best noise performance for on-overlap mode.

The critical capacitance, C_{conv}, at which the conversion gain drops is approximately given by (18) as can be seen in Fig. 4. The critical capacitance for the filtering of cyclostationarity, *i.e.*, C_{cyclo}, is given by :

$$C_{cyclo} \approx \frac{g_0}{2\pi \times 2f_{LO}} \tag{19}$$

Due to the difference between C_{conv} and C_{cyclo}, RF-port-referred noise drops up to a certain point with the attenuation of the cyclostationarity as seen in Fig. 6. The reduction rate in the RF-port-referred noise represents the importance of cyclostationarity. As stated earlier and can be seen in Fig. 6, the off-overlap switching shows the highest level of cyclostationarity. The RF-port-referred noise stays constant for capacitances in excess of a certain critical value as the filtering for noise and conversion gain occurs at the same rate after the capacitance reaches C_{conv}. Thus, there is an optimum capacitance in the on-overlap switching mode, which minimizes the input-referred RF-port noise and maximizes conversion gain. This capacitance is around 10pF in this example as seen in Fig. 4(a) and 6(a).

This implies that optimum S/N ratio can be obtained by operating the mixer in the on-overlap mode despite its inferior conversion gain as shown in Fig. 4. If on-overlap switching is used, (17) can be safely used as a first-order noise approximation. In addition, the on-overlap switching also improves the linearity of the mixer as mentioned in [5].

Capacitance	off-overlap		zero-overlap		on-overlap	
	S_{v0}	S_{avg}	S_{v0}	S_{avg}	S_{v0}	S_{avg}
30fF	13.3	86.0	8.12	15.5	4.60	4.78
100fF	13.3	43.9	8.12	13.5	4.60	4.78
1pF	13.3	17.2	8.12	9.9	4.60	4.75
3pF	13.2	13.9	8.11	8.6	4.60	4.67

Table 1 : f_{LO}=190MHz, f_{RF}=200MHz. IF-port PSD (unit : $10^{-18}v^2/Hz$). $S_{v0} \equiv S_{v0}(f_{IF})$. $S_{avg} \equiv < S_v(f_{IF}, t) >$

4.2. f_{LO}=2.24GHz, f_{RF}=2.44GHz, and f_{IF}=200MHz

The conversion gain obtained from (6) for various capacitors is depicted in Fig. 4(b). The critical capacitance at which the conversion gain begins decreasing with further increase of capacitance values is lower in this higher frequency operation example since the effective 3dB frequency approach $2\pi f_{IF}$ faster for higher operation frequencies.

Although similar trends as the previous example can be observed, the difference between $S_{v0}(f_{IF})$ and $< S_v(f_{IF}, t) >$ is not as conspicuous for the same capacitance as seen in Table 2, since the cyclostationarity for a given capacitance at higher frequencies is subject to more filtering, resulting in lower noise. The RF-port-referred PSD is depicted in Fig. 6(b) as a function of capacitance, suggesting that the on-overlap switching result in the best noise performance. The optimal capacitance for minimum input-referred noise and maximum conversion gain is close to 1pF in this example as seen in Fig. 4(b) and 6(b).

Capacitance	off-overlap		zero-overlap		on-overlap	
	S_{v0}	S_{avg}	S_{v0}	S_{avg}	S_{v0}	S_{avg}
30fF	13.3	24.6	8.12	11.5	4.60	4.78
100fF	13.3	16.4	8.12	9.62	4.59	4.75
300fF	13.0	13.5	8.06	8.41	4.58	4.66
500fF	12.5	12.5	7.93	8.07	4.56	4.59

Table 2 : f_{LO}=2.24GHz, f_{RF}=2.44GHz. IF-port PSD (unit : $10^{-18}v^2/Hz$). $S_{v0} \equiv S_{v0}(f_{IF})$. $S_{avg} \equiv < S_v(f_{IF}, t) >$

4.3. Simulation Consideration

Our numerical simulator for noise calculation from (16) utilizes simple trapezoidal integration algorithms and it takes about 10-minutes to calculate $< S_v(f_{IF}, t) >$ in the worst case. The more general equation (14) can be easily incorporated into a circuit simulator such as *SPICE* and noise can be efficiently calculated during transient analysis for deterministic signals.

5. CONCLUSION

Complete analysis of cyclostationary mixer noise in the presence of parasitic and load capacitances utilizing stochastic differential equations is introduced. The time-varying PSD at f_{IF} provides useful design insights, including the optimal load capacitance and the optimal switching mode to obtain minimum input-referred noise and maximum conversion gain at the same time. This analysis provides an effective and accurate simulation method which can be easily incorporated into the transient analysis of circuit simulators.

6. REFERENCES

[1] C. D. Hull and R. G. Meyer, "A Systematic Approach to the Analysis of Noise in Mixers," *IEEE Trans. Circ. and Syst.-1:Fund. Theory Appl.*, vol. 40, no. 12, Dec. 1993.

[2] M. T. Terrovitis and R. G. Meyer, "Noise in Current-Commutating CMOS Mixers," *IEEE J. Solid-State Circ.* vol. 34, no. 6, June 1999.

[3] W. Yue and B. H. Leung, "Noise Analysis for Sampling Mixers Using Stochastic Differential Equations," *IEEE Trans. Circ. and Syst.-2:Analog and Digital Signal Proc.*, vol. 46, no. 6, June 1999.

[4] D. Ham and A. Hajimiri, "Cyclostationary Noise Analysis of Mixer Noise Using Stochastic Differential Equations", *Tech. Report*, Caltech, Oct. 1999.

[5] A. R. Shahani, D. K. Shaeffer, and T. H. Lee, "A 12-mW Wide Dynamic Range CMOS Front-End for a Portable GPS Receiver," *IEEE J. Solid-State Circ.*, vol. 32, no. 12, Dec. 1997.

[6] P. Ritger and N. Rose, *Differential Equations with Applications*, McGraw-Hill, 1968.

[7] A. Hajimiri and T. H. Lee, "A General Theory of Phase Noise in Electrical Oscillators," *IEEE J. Solid-State Circ.*, vol. 33, no. 2, Feb. 1998.